Dalton Transactions

Cite this: *Dalton Trans.*, 2012, **41**, 546

www.rsc.org/dalton

PAPER

Solution behavior of iron(III) and iron(II) porphyrins in DMSO and reaction with superoxide. Effect of neighboring positive charge on thermodynamics, kinetics and nature of iron-(su)peroxo product†

K. Duerr,[a] O. Troeppner,[a] J. Olah,‡[b] J. Li,[a] A. Zahl,[a] T. Drewello,[a] N. Jux,[a] J. N. Harvey[b] and I. Ivanović-Burmazović*[a]

Received 12th August 2011, Accepted 26th September 2011
DOI: 10.1039/c1dt11521a

The solution behavior of iron(III) and iron(II) complexes of 5^4,10^4,15^4,20^4-tetra-*tert*-butyl-5,10,15,20-tetraphenylporphyrin (H_2tBuTPP) and the reaction with superoxide (KO_2) in DMSO have been studied in detail. Applying temperature and pressure dependent NMR studies, the thermodynamics of the low-spin/high-spin equilibrium between bis- and mono-DMSO Fe^{II} forms have been quantified ($K_{DMSO} = 0.082 \pm 0.002$ at 298.2 K, $\Delta H^\circ = +36 \pm 1$ kJ mol^{-1}, $\Delta S^\circ = +101 \pm 4$ J K^{-1} mol^{-1}, $\Delta V^\circ = +16 \pm 2$ cm^3 mol^{-1}). This is a key activation step for substitution and inner-sphere electron transfer. The superoxide binding constant to the iron(II) form of the studied porphyrin complex was found to be $(9 \pm 0.5) \times 10^3$ M^{-1}, and does not change significantly in the presence of the externally added crown ether in DMSO $(11 \pm 4) \times 10^3$ M^{-1}. The rate constants for the superoxide binding ($k_{on} = (1.30 \pm 0.01) \times 10^5$ M^{-1} s^{-1}) and release ($k_{off} = 11.6 \pm 0.7$ s^{-1}) are not affected by the presence of the external crown ether in solution. The resulting iron(II)-superoxide adduct has been characterized (mass spectrometry, EPR, high-pressure UV/Vis spectroscopy) and upon controlled addition of a proton source it regenerates the starting iron(II) complex. Based on DFT calculations, the reaction product without neighboring positive charge has iron(II)-superoxo character in both high-spin side-on and low-spin end-on forms. The results are compared to those obtained for the analogous complex with covalently attached crown ether, and more general conclusions regarding the spin-state equilibrium of iron(II) porphyrins, their reaction with superoxide and the electronic structure of the product species are drawn.

Introduction

Activation of molecular oxygen by an iron(II) center within heme-containing enzymes (cytochrome P450, NO synthase, cytochrome oxidase)[1] proceeds through the formation of the one-electron reduced form of the iron(II)-dioxygen adduct, $\{Fe–O_2\}^-$, which is widely accepted as an iron(III)-peroxo species.[2] The same species can be obtained in the reaction between heme iron(II) and superoxide (O_2^-). Due to its transient character and inherent low stability, its characterization could only be achieved at subzero temperatures, both in enzymatic and porphyrin model systems.[2,3] Even more difficult is the trapping and characterization of a monoprotonated iron(III)-hydroperoxo form, which is a short-lived intermediate on a way to an iron(IV)-oxo species, which results from O–O bond cleavage assisted by a second protonation step involving the same (distal) oxygen atom. Preparation of the iron(III)-hydroperoxo complex has been recently reported by using a porphyrin system with covalently linked axial imidazole (Im).[4] The axial imidazole ligation seems to be important for the formation of a metastable hydroperoxo species, because in a concerted fashion with the proton transfer it assists in the spin state and binding mode switch, from high-spin side-on to a low-spin end-on configuration (pathway (a), Scheme 1).[4]

We have also observed that the axial ligation influences the nature of a heme iron-dioxygen species and controls the mechanism of its formation.[5] These findings were obtained by studying the reaction of superoxide in DMSO with an iron complex of a crown ether-porphyrin conjugate (H_2Porph), which is also able to chelate the potassium cation.[5] There we have shown that axial coordination of DMSO alone causes not only a spin-state and

[a]*Department of Chemistry and Pharmacy, University of Erlangen-Nürnberg, Egerlandstr. 1, 91058, Erlangen, Germany. E-mail: ivana.ivanovic@chemie.uni-erlangen.de*
[b]*School of Chemistry and Centre for Computational Chemistry, University of Bristol, Cantock's Close, Bristol, UK, BS8 1TS*

† Electronic supplementary information (ESI) available: Spectroelectrochemistry, effect of temperature and pressure on the equilibrium constant K_{DMSO}, ESI mass spectrometry, EPR spectroscopy kinetics and thermodynamics of superoxide binding, high-pressure UV/vis measurements, DFT calculations. See DOI: 10.1039/c1dt11521a

‡ Present address: Department of Inorganic and Analytical Chemistry and Materials Structure and Modeling Research Group of the Hungarian Academy of Sciences, Budapest University of Technology and Economics, P.O. Box 91, 1521 Budapest, Hungary.

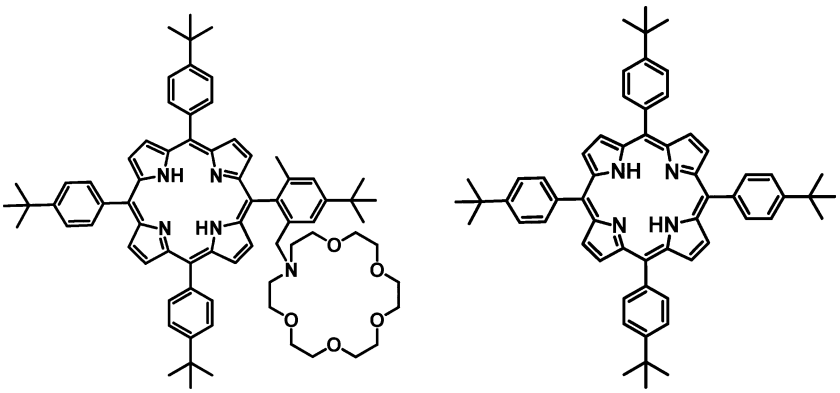

H_2Porph H_2tBuTPP

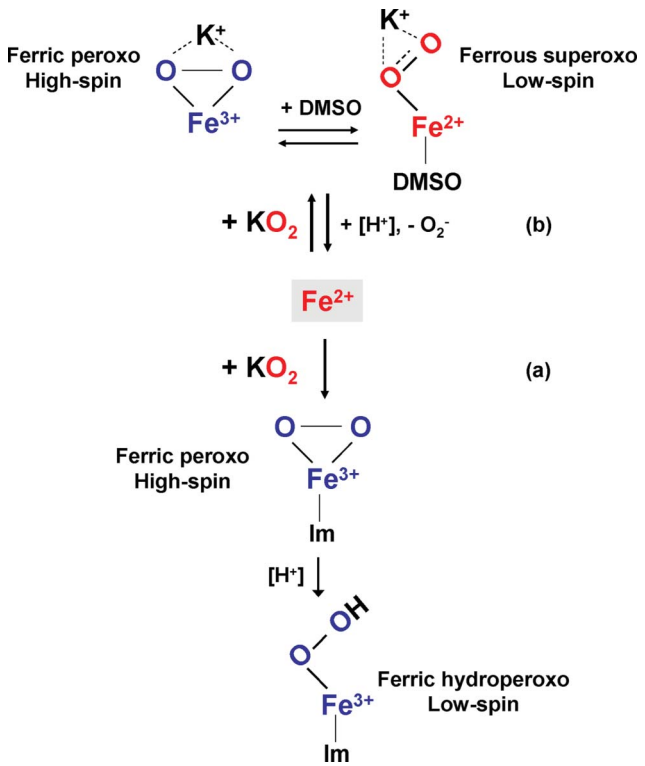

Scheme 1 Products of the superoxide reaction with heme Fe(II) and subsequent fine tuned protonation: (a) heme species with the covalently linked axial imidazole ligand,[4] (b) heme species with the covalently linked potassium cation moiety.[5]

binding-mode switch of heme peroxide but also a redox-state switch, resulting in the co-existence of two isomeric forms in equilibrium, *viz*. Fe(II)-superoxo and Fe(III)-peroxo (pathway (b), Scheme 1).[5b,c] The presence of nearby K^+ seemed to be crucial for the remarkably high stability of the iron-(su)peroxo complex that was stable even at room temperature. Aided by its stability we have been able to demonstrate that binding of superoxide to the iron(II) center is a reversible process and we could quantify the kinetics and thermodynamics of O_2^- binding.[5a,c] Interestingly, addition of a controlled amount of proton sources to the reaction mixture has not resulted in either formation of Fe(III)-hydroperoxo or O–O bond cleavage and formation of a high-valent oxo-iron species. Instead, it pulled the reaction equilibrium back to the iron(II) form by decomposing the excess of superoxide present in solution (pathway (b), Scheme 1).

The arising question is whether findings such as reversible superoxide binding, high stability of the obtained iron-(su)peroxo porphyrin, the equilibrium between Fe(II)-superoxo and Fe(III)-peroxo species and generation of the Fe(II) form upon proton addition are unique features of this particular complex, caused by the presence of the nearby positive charge from the K^+-crown ether moiety. To answer this question the current study investigates the iron complex of the corresponding porphyrin without covalently attached crown ether moiety (H_2tBuTPP) and the reaction of the Fe(II) form with superoxide (KO_2) in DMSO. The reaction has also been studied in the presence of externally added crown ether (18-crown-6) in order to compare its effects with those of covalently attached crown ether. To obtain insight into the influence of the positively charged surrounding on the nature of the product heme iron-(su)peroxo species, computational DFT studies have been performed as well.

Experimental

Materials and general considerations

Reagents and solvents were obtained from commercial sources and were of reagent quality unless otherwise stated. DMSO and acetonitrile were purchased as extra-dry solvents. All chemicals were used as received without further purification. $K^{18}O_2$ was prepared according to a published method;[6] $^{18}O_2$ was obtained from Aldrich.

H_2tBuTPP

The H_2tBuTPP (5^4,10^4,15^4,20^4-tetra-*tert*-butyl-5,10,15,20-tetraphenylporphyrin) ligand was obtained as a side product in the synthesis of a precursor of H_2Porph (5^2-*N*-(4-aza-18-crown-6)methyl-5^4,10^4,15^4,20^4-tetra-*tert*-butyl-5^6-methyl-5,10,15,20-tetraphenylporphyrin).[5a]

[Fe^{III}(tBuTPP)Cl]

H_2tBuTPP (300 mg, 0.357 mmol) was dissolved in 30 mL of $CHCl_3$. An $FeCl_2$ solution (67.0 mg, 0.524 mmol) in 30 mL of ethanol was added. Two drops of 2,6-lutidine were added and the solution refluxed for 2 h. Completion of the reaction was

followed by thin layer chromatography on Al_2O_3 plates, which is indicated by disappearance of the fluorescence of the free base porphyrin. After that, the mixture was filtered and worked up by shaking with water and half concentrated HCl. The organic layer was dried over anhydrous $MgSO_4$ and the solvent removed. The product is a brown powder in 84% yield. ^{1}H NMR (400 MHz, $CDCl_3$, 25° C): δ [ppm] 80.9 (br s, 8H, β-pyrr.), 13.7 (s, 4H, *m*-ArH), 12.5 (s, 4H, *m*-ArH), 7.50 (s, 4H, *o*-ArH), 2.51 (s, 36H, Ar-*t*-Bu). ^{13}C NMR (100 MHz, $CDCl_3$, 25° C): δ [ppm] 145.0 (4C, *m*-ArCH), 140.7 (4C, *m*-ArCH), 37.7 (4C, *t*-BuC^q), 29.6 (12C, *t*-Bu-CH_3). FAB-MS: *m*/*z* 892 (M^+ – Cl). UV/Vis (CH_2Cl_2): λ [nm] (ε [L cm^{-1} mol^{-1}]) 381 (54100), 419 (114000), 512 (12400), 585 (2470), 615 (5640). IR (KBr): $\tilde{\nu}$ [cm^{-1}] 2960, 2926, 2866, 1495, 1461, 1395, 1363, 1333, 1267, 1202, 1109, 1069, 998, 805, 721. Elemental analysis for $C_{60}H_{60}ClFeN_4 \cdot 3H_2O$. Calc.: C, 73.35; H, 6.77; N, 5.70. Found: C, 73.30; H, 6.95; N, 5.40%.

[Fe^{III}(tBuTPP))$_2$O]

The μ-oxo-dimer was prepared by shaking a solution of [Fe^{III}(tBuTPP)Cl] (100.0 mg, 0.119 mmol) in CH_2Cl_2 (20 mL) with a 2 M solution of aqueous NaOH (20 mL). The organic layer was separated and dried over anhydrous $MgSO_4$, and the solvent was evaporated. A brown solid was obtained in 79% yield. ^{1}H NMR (400 MHz, $CDCl_3$, 25° C): δ [ppm] 13.3 (s, 16H, β-pyrr.), 7.76 (s, 8H, *m*-ArH), 7.65 (s, 8H, *o*-ArH), 1.67 (s, 72H, Ar-*t*-Bu). ^{13}C NMR (100 MHz, $CDCl_3$, 25° C): δ [ppm] 150.3 (8C, *p*-ArC^q), 144.2 (16C, α-pyrr.); 142.1 (8C, ArC^q), 134.3 (16C, *o*-ArCH), 131.7 (16C, β-pyrr.), 123.3 (16C, *m*-ArCH), 119.9 (8C, *meso*-C), 34.5 (8C, *t*-BuC^q), 31.8 (24C, *t*-Bu-CH_3). FAB-MS: *m*/*z* 1802 (M^+) 892 (M^+ – O – FetBuTPP). UV/Vis (CH_2Cl_2): λ [nm] (ε [l cm^{-1}mol^{-1}]) 418 (194000), 513 (11800), 575 (2980). UV/Vis (DMSO): λ [nm] 417, 560 sh, 574, 613. IR (KBr): $\tilde{\nu}$ [cm^{-1}] 2962, 2926, 2867, 1496, 1461, 1396, 1363, 1340, 1267, 1203, 1109, 1070, 999, 895, 876, 812, 799, 719.

[Fe^{III}(tBuTPP)(DMSO)$_2$]$^+$

A solution of [Fe^{III}(tBuTPP)Cl] in DMSO yields the bis-DMSO complex of the iron porphyrin. UV/Vis (DMSO): λ [nm] (ε [L mol^{-1} cm^{-1}]) 404sh (15400), 419 (17600), 496sh (3850), 535 (4000), 719 (2095).

[Fe^{III}(tBuTPP)OH]

Addition of water or NaOH to a solution of [Fe^{III}(tBuTPP)-(DMSO)$_2$]$^+$ yields the hydroxo complex [Fe^{III}(tBuTPP)OH]. UV/Vis (DMSO): λ [nm] (ε [L mol^{-1} cm^{-1}]): 416sh (14900), 438 (30600), 540 (3100), 573 (1400).

[Fe^{II}(tBuTPP)(DMSO)$_{1,2}$]

The reduced form of [Fe^{III}(tBuTPP)Cl] could be obtained by chemical reduction or bulk electrolysis. Chemical reduction in dry DMSO was achieved by using sodium dithionite (saturated solution) as reductant. UV/Vis (DMSO): λ [nm] (ε[L mol^{-1} cm^{-1}]): 411sh (12500), 430 (69750), 533 (3100). ^{1}H NMR (reduction with sodium dithionite, 300 MHz, DMSO-d_6, 25 °C): δ [ppm] 13.0 (br s, mono-DMSO pyrr.), 9.90 (s, bis-DMSO pyrr.), 8.13 (s, bis-DMSO *o*-phenyl), 7.86 (s, bis-DMSO *m*-phenyl), 3.34 (s, bis-DMSO *t*-Bu), 1.60 (s, mono-DMSO *t*-Bu).

K[Fe^{III}(tBuTPP)(O_2^{2-})]

KO_2 was suspended in a solution of [Fe^{III}(tBuTPP)Cl] in dry DMSO. The solution was stirred until the color changed to green and was filtered under argon atmosphere. UV/Vis (DMSO): λ [nm] (ε [L mol^{-1} cm^{-1}]): 422sh (36100), 439 (148000), 568sh (6900), 612 (3710).

Equipment

Elemental analysis was carried out on a HERAEUS CHN-Mikroautomat, a Euro EA 3000 (Euro Vector) and an EA 1108 (Carlo Erba) instrument. L-SIMS (Cs^+) mass spectra were recorded with a Micromass ZABSpec mass spectrometer employing *m*-NBA as the matrix. Standard ^{1}H and ^{13}C NMR spectra were measured on a Bruker Avance 300 spectrometer. Standard IR spectra (KBr) were measured on a FT-IR IFS 88 spectrometer (Bruker Analytische Messtechnik GmbH).

Spectroelectrochemistry

Electrochemical reduction was performed under nitrogen at a Pt mesh working electrode with an Ag wire pseudo-reference electrode and a platinated Ti auxiliary electrode separated from the working electrode compartment by a glass frit. The experiment was stopped when no further change in the UV/Vis spectra was observed. Time-resolved UV/Vis spectra were taken by a UV/Vis immersion probe (Hellma 661.502-QX quartz suprasil). It was attached *via* optical cables to a 150 W Xe lamp. Recording of the spectra was done by a multi-wavelength J & M detector. An Autolab instrument with a PGSTAT 30 was used as potentiostat.

^{1}H NMR investigation of [Fe^{II}(tBuTPP)(DMSO)$_n$] (*n* = 1, 2)

Sample preparations were done in an Ar MBraun glovebox. A sample of [Fe^{II}(tBuTPP)(DMSO)$_n$] (*n* = 1, 2) was prepared by addition of an excess of $Na_2S_2O_4$ to a 2 mM solution of [Fe^{II}(tBuTPP)(DMSO)$_n$] (*n* = 1, 2) in dry DMSO-d_6. The suspension was stirred for 30 min. ^{1}H NMR spectra were taken after filtration.

Temperature-dependent NMR spectra in DMSO-d_6 were measured on a Bruker Avance 300 or Bruker AVANCE DRX 400WB instrument. All spectra were recorded in 5 mm o.d. NMR tubes, and chemical shifts were reported as δ (ppm) values calibrated to natural abundance deuterium solvent peaks (ppm).

A homemade high-pressure probe described in the literature was used for the variable-pressure experiments.[7] Pressure-dependent measurements were performed in a standard 5 mm NMR tube cut to a length of 50 mm. To enable pressure transmittance to the solution, the NMR tube was closed with a moveable KEL-S piston. The advantage of this method is that oxygen-sensitive samples can be easily placed in the NMR tube and sealed with the KEL-S piston under argon atmosphere. A safe subsequent transfer to the high-pressure probe is assured. The pressure was applied to the high-pressure probe *via* a perfluorinated hydrocarbon pressure medium (hexafluoropropylene oxide, Hostinert 175, Hoechst) and measured by a VDO gauge with an accuracy of 1%. The

temperature was adjusted with circulating, thermostated water (Colora thermostat WK 16) to 0.1 K of the desired value and monitored before each measurement with an internal Pt-resistance thermometer with an accuracy of 0.2 K.[8] The temperature was chosen to be 320 K and kept constant, since at lower temperatures DMSO can freeze upon increasing the pressure.

ESI and cryospray mass spectrometry

Using a syringe pump at a flow rate of 240 mL h^{-1}, the DMSO solutions were infused into an orthogonal ESI source of an Esquire 6000 ion trap mass spectrometer (Bruker, Bremen, Germany). Nitrogen was used as the nebulizing gas at a pressure of 10 psi and as the drying gas at a temperature of 300° C and a flow rate of 5 L min^{-1}. The ion trap was optimized for the respective target mass of the ions under investigation. The source voltages varied with this optimization. All experiments were carried out in the positive-ion mode. The sample of the starting complex [Fe^{III}(tBuTPP)Cl] was prepared by making a 5×10^{-4} M suspension in dry DMSO (stirred overnight) under nitrogen and subsequent filtration. Other samples were prepared by dissolving excess of either KO_2 or $K^{18}O_2$ in an overnight-prepared 5×10^{-4} M suspension of [Fe^{III}(tBuTPP)Cl] in dry DMSO under nitrogen and subsequent filtration. High mass accuracy ESI spectra were recorded on an ultra high-resolution ESI-Time-Of-Flight MS, a Bruker Daltoniks (Bremen, Germany) Maxis, which also was coupled to the Bruker cryospray. For the cryospray measurements samples were dissolved in a MeCN–DMSO (70 : 30) mixture.

Thermodynamics and kinetics

Solution preparations of KO_2, [Fe^{II}(tBuTPP)$(DMSO)_n$] (n = 1, 2) and [Fe^{III}(tBuTPP)(O_2^{2-})]$^-$ in DMSO without 18-crown-6 were done according to our previous study.[5] Solutions of [Fe^{III}(tBuTPP)(O_2^{2-})]$^-$ in DMSO with 18-crown-6 were prepared by addition of a ten-fold excess of 18-crown-6 (relative to the porphyrin concentration) to a freshly prepared solution of [Fe^{II}(tBuTPP)$(DMSO)_n$] (n = 1, 2).

A Hewlett-Packard 8452A spectrophotometer was used for qualitative UV/Vis measurements and measurement of the binding constant of superoxide to [Fe^{II}(tBuTPP)$(DMSO)_n$] (n = 1, 2) without and with added 18-crown-6 (10 times the concentration of the porphyrin complex).

A spectrophotometric study of the binding of superoxide to [Fe^{II}(tBuTPP)$(DMSO)_n$] (n = 1, 2) was performed in a 1-cm path length cuvette with a 25 mL reservoir under nitrogen. The 1.3×10^{-5} M solution (5 mL) of electrochemically generated [Fe^{II}(tBuTPP)$(DMSO)_n$] (n = 1, 2) was titrated with aliquots of a saturated KO_2 solution in DMSO added from a Hamilton microsyringe. The same experiment was performed with the Fe(II) complex and added 18-crown-6 (1.3×10^{-5} M and 1.3×10^{-4} M, respectively). Data were fitted according to following equation (A_0 and A_∞ represent the absorbance at 0 and 100% of the product formation, respectively, A_x represents the absorbance at the respective measured superoxide concentration):[9]

$$A_x = A_0 + (A_\infty - A_0)K[O_2^-]/(1 + K[O_2^-])$$

Kinetic data were obtained by recording time-resolved UV/Vis spectra using a modified μSFM-20 Bio-Logic stopped-flow module combined with a Huber CC90 cryostat or a Biologic SFM-400 four syringes stopped-flow system (using only the first three syringes) and a high density mixer to minimize mixing effects in DMSO solutions. The stopped-flow set-ups were equipped with a J&M TIDAS high-speed diode array spectrometer with combined deuterium and tungsten lamps (200–1015 nm wavelength range). Isolast O-rings were used for all sealing purposes to enable measurements in DMSO, and solutions were delivered from 10 mL gas-tight Hamilton syringes. The syringes were controlled by separate drives, allowing for variation of the ratio of mixing volumes used in the kinetic runs. Data were analyzed using the integrated Bio-Kine software version 4.23 and also the Specfit/32™ program. At least five kinetic runs were recorded under all conditions, and the reported rate constants represent the mean values. The stopped-flow instrument was thermostated to the desired temperature ±0.1 °C. Experiments at 25 °C were performed in DMSO solution. All kinetic measurements were carried out under pseudo-first-order conditions; *i.e.* superoxide concentration was in large excess (complex concentration was usually 5×10^{-6} M). The reactions were studied at an ionic strength of 0.1 M (Bu_4NPF_6).

For the rapid kinetic measurements, the Bio-Logic stopped-flow module was upgraded to a submillisecond mixing stopped-flow configuration by combining it with a microcuvette accessory (with an optical pathlength of 0.8 mm) and a monochromator to minimize the dead time of the instrument.[10]

High-pressure UV/Vis measurements

Sample preparation was carried out in an Ar MBraun glovebox. A sample of [Fe^{III}(tBuTPP)(O_2^{2-})]$^-$ was prepared by addition of an excess of KO_2 to a 10^{-5} M solution of [Fe^{III}(tBuTPP)Cl] in a dry DMSO solution of 0.1 M TBAP. The suspension was stirred for 30 min. High pressure UV/Vis spectra were recorded after filtration.

Spectral measurements at elevated pressure were performed in a pill-box cuvette on a Shimadzu UV-2101-PC spectrophotometer using a home-made high-pressure cell.[11] The high-pressure pump was purchased from NOVA SWISS (Nova Werke AG, CH-8307 Effretikon, Vogelsangstrasse); it allows measurements up to 150 MPa.

DFT calculations

Geometry optimizations of the structures were performed with the Jaguar 6.0 program package[12] using the B3PW91 and B3LYP functionals, and a restricted open shell formalism (ROKS). The 6-31G(d) basis set was used on all atoms with the exception of the metal ions for which the standard Los Alamos effective core potentials[13] were used with the associated double-ζ, basis LACVP on potassium and the triplet-ζ basis LACV3P[14] on iron. The calculated total energies of the optimized structures *in vacuo*, together with the total energy of the dissociated DMSO ligand, were used to compare the stability of the side-on and end-on complexes.

Results and discussion

In a DMSO solution Fe(III) porphyrins exist as bis-DMSO species.[15] Similar to the [Fe^{III}(Porph)$(DMSO)_2$]$^+$ complex

with the covalently attached crown ether moiety,[5] the $[Fe^{III}(tBuTPP)(DMSO)_2]^+$ complex reacts with an excess of KO_2 resulting in an adduct commonly described as $[Fe^{III}(tBuTPP)(O_2^{2-})]^-$.[2] The reaction proceeds in two steps. In the first step Fe(III) is reduced to Fe(II), which in the second step binds superoxide yielding $[Fe^{III}(tBuTPP)(O_2^{2-})]^-$.[2,5] In this study we used the electrochemically generated Fe(II) form of the complex as the reactant, *i.e.* we concentrated on the second reaction step. As previously reported,[5a] the first reaction step, reduction of the Fe^{III} to the Fe^{II} porphyrin complex by KO_2, could not be quantitatively studied in detail because of interference of the Fe(III)-hydroxo species formation by KOH, which is inevitably present in commercial KO_2. Details on the spectroelectrochemical measurements and UV/vis characterization of different Fe(III) forms of the studied complex are given in ESI† (Fig. S1–S4, Table S1 and Scheme S1)

^{1}H NMR investigation of $[Fe^{II}(tBuTPP)(DMSO)_n]$ (n = 1, 2)

Solvation of iron(II) tetraphenylporphyrins in DMSO leads to an equilibrium between mono- and bis-DMSO complexes (Scheme 2).[5,16] In order to investigate the thermodynamics of such equilibrium in the case of $[Fe^{II}(tBuTPP)(DMSO)_n]$, temperature- and pressure-dependent ^{1}H NMR studies were performed.

$$[Fe^{II}(tBuTPP)(DMSO)_2] \underset{}{\overset{K_{DMSO}}{\rightleftharpoons}} [Fe^{II}(tBuTPP)(DMSO)] + DMSO$$

LS; S = 0 HS; S = 2

$$K_{DMSO} = [HS]/[LS]$$

Scheme 2

Literature data on NMR of $[Fe^{II}(tpp)]$ in DMSO reveal the co-existence of high-spin and low-spin species[16] with a moderately broad paramagnetic signal of the pyrrole protons at around 12 ppm. This finding corresponds to the NMR spectra of investigated $[Fe^{II}(tBuTPP)(DMSO)_n]$ (n = 1, 2) (Fig. S5, ESI†). In the region from 0 to 10 ppm, there are signals with only minor line broadening which correspond to the signals of the diamagnetic $[Fe^{II}(tBuTPP)(DMSO)_2]$ species. The broad signal at around 13 ppm belongs to the resonances of the pyrrole protons of the paramagnetic $[Fe^{II}(tBuTPP)(DMSO)]$ species. The remaining paramagnetic resonances cannot be observed as they are merged with the diamagnetic ones (Fig. S5, ESI†). The position and line broadening of the pyrrole protons of a porphyrin system are generally used in order to determine the spin state of the central metal.[17]

Upon increase of temperature the paramagnetic signal shifts strongly to lower field (Fig. S6, ESI†). The remainder of the spectrum remains almost unchanged. Line broadening increases only moderately. After letting the sample cool down, the starting spectrum is retrieved. This supports the existence of the high-spin/low-spin equilibrium, with the share of the high spin species increasing with the temperature increase.

Since the low-spin/high-spin equilibrium constant (K_{DMSO}, Scheme 2) should also be pressure sensitive, we performed pressure-dependent ^{1}H NMR measurements. A pressure increase shows a shift of the equilibrium to the diamagnetic low-spin species (Fig. 1). This is expected, since a higher pressure favors the

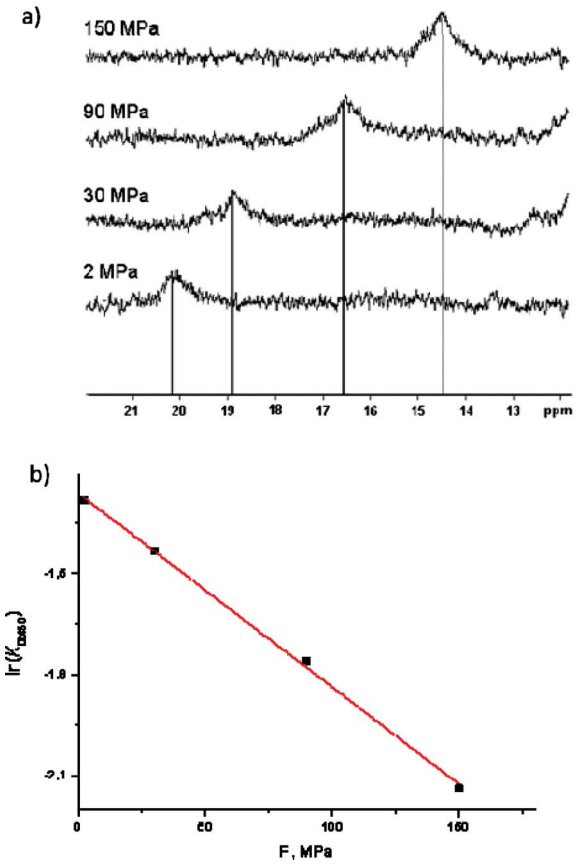

Fig. 1 (a) ^{1}H NMR spectrum of $[Fe^{II}(tBuTPP)(DMSO)_n]$ (n = 1, 2) at 325.2 K and different pressures; (b) plot of $\ln(K_{DMSO})$ *vs.* pressure.

coordination of the second DMSO molecule. Decrease of pressure after the experiment shows again a larger share of the high-spin species and confirms the reversibility of the observed pressure dependent process.

The temperature- and pressure-dependent measurements enable the quantification of the thermodynamic parameters for the equilibrium K_{DMSO} in Scheme 2 (HS = high-spin mono-DMSO complex; LS = low-spin bis-DMSO complex; the activity of solvent is considered to be 1). The parameters are summarized in Table 1 (for details see Supplementary Information and Table S2, ESI†).

The temperature dependence plot of $\ln(K_{DMSO})$ (Fig. S7, ESI†) was found to be linear and resulted in significantly positive values for the thermodynamic parameters $\Delta H°$ and $\Delta S°$ (Table 1). They are in agreement with the endothermic and dissociative character of the underlying low-spin to high-spin transition. Interestingly, the spin-state equilibrium in the case of ferric cytochrome P450 is characterized within the corresponding temperature range by similar thermodynamic parameters ($\Delta H°$ = +42 kJ mol^{-1} and

Table 1 Thermodynamic parameters for the equilibrium constant K_{DMSO}

K_{DMSO} at 298.2 K	0.082 ± 0.002
$\Delta H°$/kJ mol^{-1}	+36 ± 1
$\Delta S°$/J K^{-1} mol^{-1}	+101 ± 4
$\Delta G°$/kJ mol^{-1} at 298.2 K	6 ± 1
$\Delta V°$/cm^3 mol^{-1} at 325.2 K	+16 ± 2

ΔS° = +152 J K^{-1} mol^{-1}).[18] A typical entropy change that is considered to drive the spin transition from low- to high-spin state is approximately 50 J K^{-1} mol^{-1}, and in the case of an Fe(II) spin-crossover compound is found to be 60 J K^{-1} mol^{-1}.[19] The observed entropy change of ~101 J K^{-1} mol^{-1} (Table 1) is significantly larger than that associated with the simple spin transition indicating that the covalent bond breaking and an increase in translational and rotational degrees of freedom as a consequence of a dissociative process have significant contribution. By way of comparison, in the opposite associative process accompanied by high-spin to low-spin transition upon CO rebinding to the five-coordinate (L)Fe^{II}4SP complexes (4SP = tetrakis(4-sulfonatophenyl)porphyrin, L = H_2O or 2-methylimidazole)) the reaction entropy were found to be −117 J K^{-1} mol^{-1}.[20]

The values of K_{DMSO} and the corresponding distribution of species (see Table S2, ESI†) show that in DMSO solution mostly the low-spin bis-DMSO complex exists (92% at 298 K and 0.1 MPa). The pressure dependence of ln(K_{DMSO}) also gave a straight line (Fig. 1b) and resulted in ΔV° = +16 ± 2 cm^3 mol^{-1}. The high positive reaction volume is a result of DMSO dissociation that accompanies the spin-state change on the Fe center. The reaction volume changes for spin transitions in Fe(II) complexes have been reported to range between 5 and 19 cm^3 mol^{-1},[19,21] whereas the covalent bond breaking contributes to a volume change with roughly 5–10 cm^3 mol^{-1}.[22] This implies that the change in coordination number on the iron center coupled to a spin-state transformation is characterised by volume changes of 10–30 cm^3 mol^{-1}. For example, CO photodissociation accompanied by low-spin to high-spin change is coupled to volume expansions of ~17 and ~12 cm^3 mol^{-1} for the above mentioned (L)Fe^{II}4SP complex and Fe^{II}MP-11 (MP-11 = microperoxidase-11), respectively.[20] Similar processes of other heme model complexes exhibit an reaction volume of ~30 cm^3 mol^{-1}.[23] On the other hand measurements of spin equilibria and ligand binding/release in the case of heme proteins typically yield volume changes of 10–50 cm^3 mol^{-1}.[24] However, the case of proteins may differ from model complexes in that the spin-state transition caused by ligand binding/release can be coupled with additional changes of the protein structure and prominent solvent reorganisation due to (de)hydration of regions outside the active site, resulting in very large volume changes (larger than 200 cm^3 mol^{-1}).[24b] Interestingly, our recent studies on the spin state equilibrium (analogue to that in Scheme 2) of the iron(II) complex of the crown ether-porphyrin conjugate,[5c] [Fe^{II}(Porph)(DMSO)$_n$] (n = 1, 2), have shown that the presence of the crown ether moiety slightly shifts the K_{DMSO} equilibrium into the direction of the low-spin bis-DMSO species (K_{DMSO} = 0.030 ± 0.001, 97% of the low-spin component at 298 K and 0.1 MPa). This strongly suggests that the covalently attached crown ether makes dissociation of the sixth ligand somewhat less favorable.[5c] The corresponding reaction enthalpy (ΔH° = +48 ± 1 kJ mol^{-1}) is more positive than that for [Fe^{II}(tBuTPP)(DMSO)$_n$], supporting the fact that the crown ether makes DMSO dissociation more endothermic. Furthermore, the significantly larger reaction volume (ΔV° = +26 ± 2 cm^3 mol^{-1})[5c] in the case of [Fe^{II}(Porph)(DMSO)$_n$] implies that DMSO release causes additional structural changes on the resulting mono-DMSO species, which involves a new orientation between the covalently attached crown ether and porphyrin plane (creating a more "open" structure) accompanied by additional solvent perturbations.

ESI mass spectrometry in DMSO

The best correlation of mass spectra with the solution chemistry of the corresponding coordination compounds is currently achieved by soft electrospray ionization (ESI). Therefore, we have used ESI for the characterization of the reactant and product species in solution.

The mass spectrum of the starting Fe(III) complex (Fig. S8, ESI†), [Fe^{III}(tBuTPP)(DMSO)$_2$]$^+$, shows a single peak at m/z 970.3, corresponding to [Fe^{III}(tBuTPP)(DMSO)]$^+$. The isotopic distribution (Fig. S9, ESI†) confirms this assignment. A collision experiment with He gas (MS/MS or tandem mass spectrometry) yields the porphyrin complex [Fe^{III}(tBuTPP)]$^+$ without axial ligands at m/z 892.4 (inset in Fig. S8, ESI†).

The reaction mixture of [Fe^{III}(tBuTPP)(DMSO)$_2$]$^+$ and KO_2 was investigated. The ESI mass spectrum of the reaction product shows the main ion peak at m/z 1002.3 corresponding to {K$^+$ + K[Fe^{III}(tBuTPP)(O_2^{2-})]} (Fig. 2). In order to confirm the peak at m/z 1002.3 as the superoxo {K$^+$ + K[Fe^{III}(tBuTPP)(O_2^{2-})]} adduct, the same experiment was repeated with a mixture of K$^{16}O_2$ and K$^{18}O_2$ (1 : 1) (inset in Fig. 2). The mass spectrum shows again the peak at m/z 1002.3 with a new one at m/z 1006.3, shifted by 4 mass units as expected for the $^{18}O_2^-$ adduct, and its elemental composition is also confirmed by the corresponding isotopic distributions (Fig. S10, ESI†).

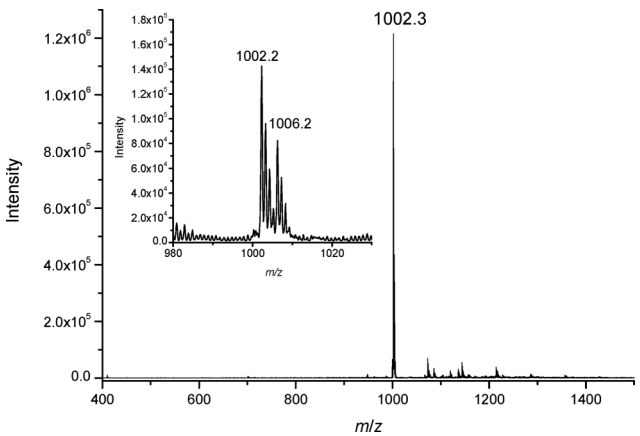

Fig. 2 Mass spectrum of {K$^+$ + K[Fe^{III}(tBuTPP)(O_2^{2-})]}. Inset: Mass spectrum of {K$^+$ + K[Fe^{III}(tBuTPP)($^{16}O_2^{2-}$)]} and {K$^+$ + K[Fe^{III}-(tBuTPP)($^{18}O_2^{2-}$)]}.

The corresponding crown ether containing species, {K$^+$ + K[Fe^{III}(Porph)(O_2^{2-})]}, was observed previously using the crown ether attached porphyrin complex.[5b] Both these ions show a distinctly different dissociation behavior in MS/MS experiments, which indicates different structural motifs. Upon collision with He gas, {K$^+$ + K[Fe^{III}(Porph)(O_2^{2-})]} shows the fragmentation into intact K[Fe^{II}(Porph)]$^+$ by the straightforward loss of KO_2. Obviously, one K$^+$ cation is coordinated with the O_2 moiety while the other K$^+$ cation resides with the crown ether. The covalently attached crown ether stabilizes the porphyrin complex as a potassium chelating agent. The MS/MS experiment of {K$^+$ + K[Fe^{III}(tBuTPP)(O_2^{2-})]} shows a more complex dissociation behavior which clearly also involves the decomposition of the porphyrin. Fragment ions are observed at m/z 984.1, 958.1, 946.2 and 825.1 (inset in Fig. S11, ESI†). These fragment ions are shifted

by two mass units to higher masses when the $^{18}O_2$-labeled $\{K^+ + K[Fe^{III}(tBuTPP)(^{18}O_2^{2-})]\}$ precursor is studied as the parent ion. Therefore, each fragment ion has lost one oxygen atom in the dissociation. A tentative assignment of the fragment ions would be H_2O loss (*m/z* 984.1), followed by loss of CN or C_2H_2 (*m/z* 958.1), followed by the loss a *tert*-butylphenyl radical (*m/z* 825.1). An MS^3 experiment confirmed the sequence: *m/z* 1002 dissociates *via* *m/z* 958 into *m/z* 825. The fragment ion at *m/z* 946.2 could correspond to the loss of KOH. In summary, the dissociations of $\{K^+ + K[Fe^{III}(tBuTPP)(O_2^{2-})]\}$ show both incorporation of one oxygen atom and fragmentation of the porphyrin moiety.

We also used a cryospray mass spectrometric technique[25] coupled to the ultra-high-resolution time-of-flight detector to allow efficient transfer of the intact species from solution-state into the gas phase. Operation on low temperatures (at −30 °C in the MeCN–DMSO (70 : 30) solvent mixture)[5a] reduces possible decomposition processes and dissociation of weakly bound ligands to a minimum. Also under these conditions, in the MS spectrum of the starting Fe(III) complex, $[Fe^{III}(tBuTPP)(DMSO)]^+$ (peak at *m/z* 970.4287) appears as a main species (Fig. S12, ESI†), whereas the spectrum of the reaction product clearly shows existence of the $\{K^+ + K[Fe^{III}(tBuTPP)(O_2^{2-})]\}$ adduct (peak at *m/z* 1002.3337) (Fig. S13, ESI†). This suggests that DMSO as the sixth ligand is quite labile, at least under the conditions of MS experiments.

Kinetics and thermodynamics

We have previously studied the kinetics and thermodynamics of the superoxide binding to the $[Fe^{II}(Porph)(DMSO)_n]$ porphyrin complex with covalently attached crown ether.[5a] In order to understand the influence of a crown ether moiety on the thermodynamics and kinetics of the iron porphyrins interaction with superoxide in DMSO, a comparative thermodynamic and kinetic study on the porphyrin without a covalently attached crown ether moiety, was carried out. Two different sets of experiments were performed: one without any crown ether and another with a ten-fold excess of deliberately added 8-crown-6 present in solution.

As mentioned above, the reaction between the iron(II) form of the complex with KO_2 was studied, which results in $[Fe^{III}(tBuTPP)(O_2^{2-})]^-$. Qualitative experiments on the stability of $[Fe^{III}(tBuTPP)(O_2^{2-})]^-$ (λ_{max} = 439 nm) were done by bubbling moist air through the complex solution in presence of excess superoxide. In analogy to the iron porphyrin complex with the covalently attached crown ether,[5a] the iron(II) complex (λ_{max} = 430 nm) is formed (Fig. S14, ESI†) due to the superoxide decomposition and shift of the equilibrium to the starting complex (Scheme 3). This shows that reversible binding of superoxide to an iron(II) porphyrin is a general feature independent of the presence of the covalently attached crown in the complex structure. The reaction and its reversibility were further thermodynamically and kinetically quantified.

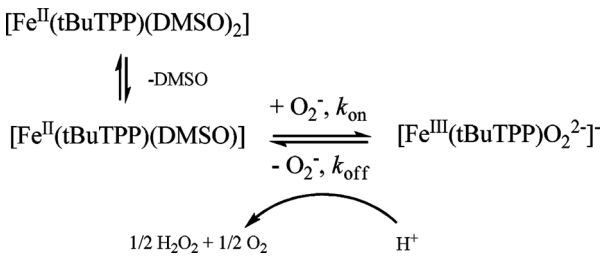

Scheme 3

The superoxide binding constant was determined by titration experiments in analogy to the previous study (Fig. S15, ESI†).[5a] The experimentally obtained value ($K = (9 \pm 0.5) \times 10^3$ M^{-1}) for the binding of superoxide to $[Fe^{II}(tBuTPP)(DMSO)_n]$ is approximately one order of magnitude lower than the corresponding value in the case of $[Fe^{II}(Porph)(DMSO)_n]$ ($K = (1.7 \pm 0.2) \times 10^5$ M^{-1}).[5a] This corresponds to our qualitative observations of $[Fe^{III}(tBuTPP)(O_2^{2-})]^-$ being less stable than its analogue with covalently attached crown ether moiety. The same experiment was done with addition of a ten-fold excess of 18-crown-6 related over the porphyrin concentration (Fig. S16, ESI†). The binding constant of $K = (11 \pm 4) \times 10^3$ M^{-1} is obtained and it is the same (within experimental error) as in the case with no external crown ether present in solution. This shows that the presence of external crown ether in the solution does not exhibit a beneficial stabilizing effect. In that way, a stabilizing effect of covalently attached crown ether on the peroxo complex could be quantified.

UV/Vis stopped-flow measurements of the reaction of $[Fe^{II}(tBuTPP)(DMSO)_n]$ (n = 1, 2) with saturated KO_2 solution in DMSO were performed. The experiment was carried out according to our previous study.[5a,25] Superoxide concentrations were varied by using saturated KO_2 solution in DMSO and varying the mixing volume ratios. The time-resolved spectra were fitted to a single-exponential function to give values for the observed rate constants k_{obs} (Fig. 3). The corresponding second-order rate constant $k_{on} = (1.30 \pm 0.01) \times 10^5$ M^{-1} s^{-1} is approximately one order of magnitude higher than in the case of the complex with covalently attached crown ether ($k_{on} = (3.65 \pm 0.05) \times 10^4$ M^{-1} s^{-1}).[5a] Such kinetic effect is most probably due to steric reasons. Considering the binding constants and the values for k_{on} for both complexes, it can be concluded that k_{off} ($k_{off} = k_{on}/K$) is approximately two orders of magnitude slower for $[Fe^{III}(Porph)(O_2^-)]^-$ ($k_{off} = 0.21 \pm 0.01$ s^{-1})[5a] than for $[Fe^{III}(tBuTPP)(O_2^-)]^-$ ($k_{off} = 14.4 \pm 0.1$ s^{-1}). By slowing down the superoxide dissociation from the metal center the crown ether moiety with coordinated K^+ stabilizes

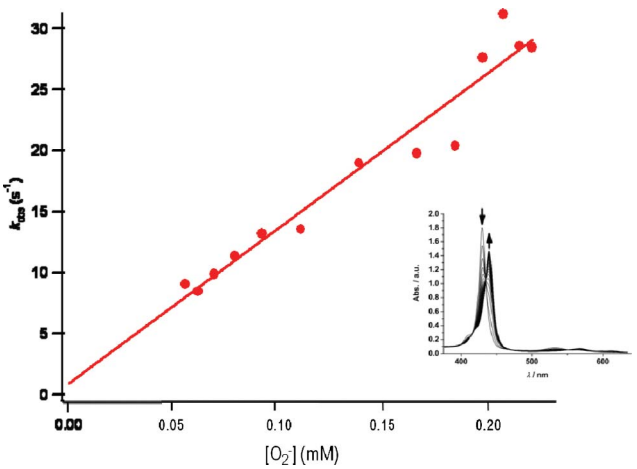

Fig. 3 Plot of k_{obs} *vs.* superoxide concentration for the reaction of 1×10^{-5} M $[Fe^{II}(tBuTPP)(DMSO)_n]$ (n = 1, 2) and KO_2 at 25° C using different mixing volume ratios (I = 0.1 M Bu_4NPF_6). Inset: Time resolved UV/Vis spectra of the reaction of complex with 0.1×10^{-3} M of KO_2.

the superoxide adduct. The assumption that the crown ether side chain prevents to some extent dissociation of the axial ligand is in agreement with somewhat higher amount of bis-DMSO species present in the K_{DMSO} equilibrium mixture (Scheme 2) in the case of [Fe^{II}(Porph)(DMSO)$_n$] (97%; $n = 1$ or 2) than in the case of the [Fe^{II}(tBuTPP)(DMSO)$_n$] system (92%; *vide supra*).

The k_{off} value have been also directly determined by adding controlled amount of a proton source (HOTf acid) into the [Fe^{III}(tBuTPP)(O_2^-)]$^-$ product solution, where an excess of KO_2 was also present. HOTf was chosen since it is known that strong acids react with superoxide in aprotic solvents extremely rapidly ($k' > 1 \times 10^7$ M^{-1} s^{-1})[26] which makes them very efficient O_2^- scavengers even at low concentrations. As shown in Scheme 3, rapid decomposition of superoxide shifts the equilibrium back to the Fe(II) form. Upon subsequent addition of superoxide to this solution the product [Fe^{III}(tBuTPP)(O_2^-)]$^-$ is fully recovered. To better visualize this process we performed experiments by using two-mixer stopped-flow system. The [Fe^{III}(tBuTPP)(O_2^-)]$^-$ complex (5×10^{-6} M) with excess of KO_2 (0.1–1 mM) was in the first syringe and mixed with the solution of HOTf (0.1–2 mM) from the second syringe (off-reaction). To the obtained product solution (after 1 s delay) additional superoxide (from the third syringe) was introduced in the second mixer (on-reaction). The corresponding time-resolved spectra, kinetic trace and speciation spectra are shown in Fig. 4. Such experiments have revealed that independent on the applied acid concentration or excess of KO_2 the formation of the Fe(II) complex proceeds in one step, without formation of any intermediate Fe(III) specie, with the corresponding first order rate constant $k_{obs} = k_{off} = 11.6 \pm 0.7$ s^{-1}. This value is in excellent agreement with that obtained based on k_{on} and the binding constant ($k_{off} = k_{on}/K$, *vide supra*).

The kinetic studies were also performed for the reaction of [Fe^{II}(tBuTPP)(DMSO)$_n$] (n = 1, 2) in the presence of a ten-fold excess of 18-crown-6 in solution. The obtained second-order rate constant (Fig. S17, Table S3, ESI†) for the formation of the peroxo complex was $k_{on} = (1.6 \pm 0.2) \times 10^5$ M^{-1} s^{-1}, which corresponds to the one obtained without added crown ether ($k_{on} = (1.30 \pm 0.01) \times 10^5$ M^{-1} s^{-1}). Having k_{on} and k_{off} (11.1 ± 0.5 s^{-1}) for the reactions in the presence of external crown-ether, the reaction equilibrium constant can be calculated $K = k_{on}/k_{off} = (14 \pm 3) \times 10^3$ M^{-1}. The obtained value is in excellent agreement with the thermodynamically estimated one ($K = (11 \pm 5) \times 10^3$ M^{-1}, *vide supra*) and with that obtained without added crown ether present in solution.

EPR

In order to shed light on the electronic nature of our Fe^{II} porphyrin superoxide adduct we performed X-band EPR measurements. However, in contrast to our previous investigations on the crown ether porphyrin system ([Fe(Porph)Cl]),[5b] due to the very low solubility of the studied [Fe(tBuTPP)Cl] complex in DMSO we were not able to obtain detailed information from those measurements. Usually the iron signals were near the detection limit and superoxide signals dominated. Moreover, due to the lower stability of the superoxo adduct of the complex without covalently attached crown ether, signals of the reaction side products, such as hydroxo and μ-oxo complexes (*vide infra*), interfered significantly.

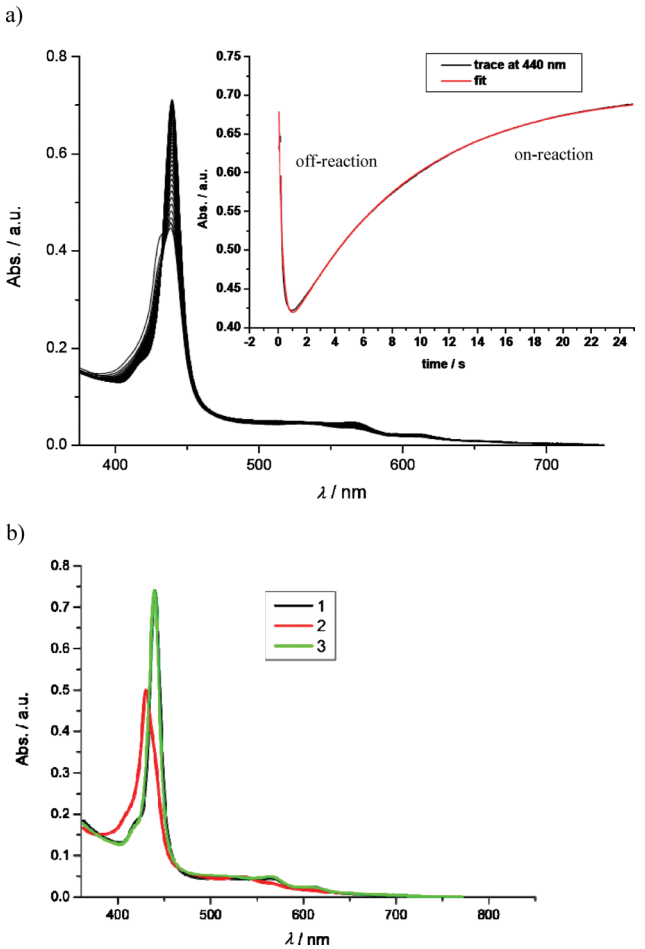

Fig. 4 (a) Time resolved UV/Vis spectra (from the experiment in the two-mixer stopped-flow) of the reaction of 5×10^{-6} M [Fe^{III}(tBuTPP)(O_2^-)]$^-$ (in the presence of 10^{-3} M KO_2) with 1 mM HOTf (in the first mixer) and subsequently with KO_2 (in the second mixer after 1 s delay; in DMSO, I = 0.1 M Bu_4NPF_6); inset: kinetic trace at 440 nm and a two-exponential fit. (b) Spectra of the species observed along the reaction path: ***1*** [Fe^{III}(tBuTPP)O_2^{2-}]$^-$, ***2*** [Fe^{II}(tBuTPP)(DMSO)$_n$] (n = 1, 2), ***3*** [Fe^{III}(tBuTPP)O_2^{2-}]$^-$.

As commercially available Na_2O_2 contains up to 10% of NaO_2, and since "naked" peroxide is not stable in aprotic solution,[27] we used it as a source of superoxide, which is released in solution by stirring of the granules in DMSO. This enables quantitative generation of iron (su)peroxo species without using a high superoxide excess (the concentration of superoxide that is present in the saturated DMSO solution of Na_2O_2 is estimated to be $(4 \pm 2) \times 10^{-5}$ M).[5b] The EPR spectrum at 12 K of the reaction product between the studied iron porphyrin and Na_2O_2 in DMSO (Fig. 5) shows only a weak signal of rhombic high-spin Fe^{III} at $g = 4.20$, characteristic for the side-on peroxo species.[2b,5b] Signals of a byproduct Fe^{III} hydroxo species ($g = 7.24$ and $g = 5.34$) are also present in the spectrum, similar to what has been observed in the case of [Fe^{III}(Porph)][5b] and other porphyrin systems.[28] The signals of the free solvated superoxide and superoxide bound to the Na^+ cation ($g = 2.10$, $g = 2.00$)[5b] are much more intense than the signals of the iron species. Thus, although the EPR spectra demonstrated the presence of both Fe^{II}–O_2^- and Fe^{III}–O_2^{2-} species of the crown ether porphyrin conjugate,[5b] evidence for the possible

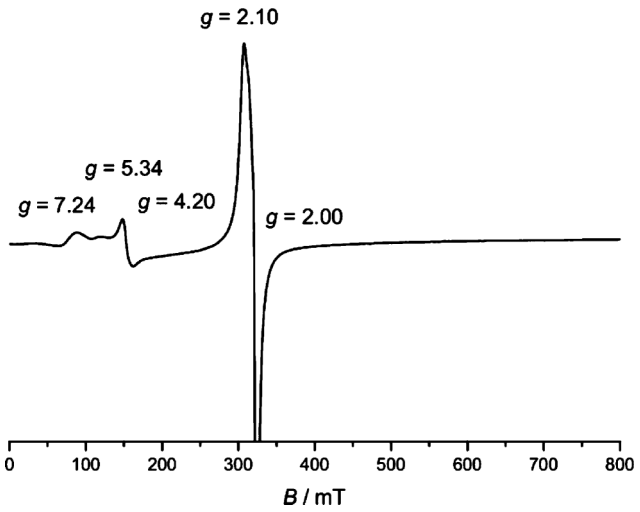

Fig. 5 X-Band EPR spectra of [Fe^{III}(tBuTPP)Cl] with Na_2O_2 in DMSO at 12 K, microwave frequency was 8.989384 GHz, P = 1 mW; modulation width = 1.0 mT, sweep width 800 mT.

superoxide coordination to iron, Fe^{II}–O_2^-, could not be found in the case of the [Fe(tBuTPP)] system. At 77 K iron signals could not be observed at all, whereas the superoxo signals showed no change in g values with temperature increase.

When KO_2 was used, higher concentrations of superoxide and hydroxide were present in solution compared to the Na_2O_2 experiment. The corresponding EPR spectrum of [Fe^{III}(tBuTPP)Cl] with KO_2 in DMSO at 12 K (Fig. S18, ESI†), besides the signals of rhombic iron(III)-peroxo (g = 4.20) and hydroxo species (g = 5.46, g = 7.32), showed a large paramagnetic signal around g = 1.99 mixed with the signal of free superoxide. It has the nature of a system with one unpaired electron.[29] It should be mentioned that μ-oxo species of iron(III) are EPR silent due to antiferromagnetic coupling.[29,30] The observed signal could be related to the formation of an iron(II)–iron(III) μ-oxo porphyrin dimer, [[Fe^{II}(tBuTPP)]–O–[Fe^{III}(tBuTPP)]]$^-$, upon decomposition of the (su)peroxo species.[30] As expected for an iron species, it is only observed at temperatures below 77 K.[30] Kadish *et al.*[30] proposed an analogous species with the TPP system and described it as a μ-oxo complex with a single electron added. The EPR spectrum of this species is very similar to the one we observe, showing one asymmetric line with g = 1.95. One can just speculate whether this species might be a hint for the existence of both iron(III)-peroxo and iron(II)-superoxo forms in solution. In the case of the complex with the covalently attached crown ether such species have not been observed, in agreement with the fact that the crown ether sterically hinders the formation of dimer complexes. At 77 K only a signal of free superoxide is observed and the other signals have vanished due to their low concentration (inset in Fig. S18, ESI†).

By using a ten-fold excess of 18-crown-6 over [Fe^{III}(tBuTPP)-$(DMSO)_2$]$^+$ a huge signal at g = 2 is observed (Fig. S19, ESI†), which upon temperature variation changes only its intensity but not the shape. The signal corresponds to superoxide bound to the potassium cation inside the crown ether and is influenced by moisture in solution.[31] In the case of iron signals only the general rhombic signal of the peroxo species around g = 4.2 can be observed (Fig. S19, ESI†).

High-pressure UV/Vis spectroscopy

Since based on the EPR spectra we were not able to get information about the possible co-existence of two isomeric forms in product solution, *viz*. Fe(II)-superoxo and Fe(III)-peroxo, we performed pressure-dependent UV/Vis measurements to probe the existence of an equilibrium state. (Due to the low complex solubility, which limited the quality of the EPR spectral data, the Mössbauer spectra of the required resolution could not be obtained as well.) The high-spin/low-spin equilibria are usually pressure sensitive and as expected the increasing pressure in the DMSO solution of the product (su)peroxide adduct causes a small but significant red-shift of the Soret absorption band (Fig. 6), indicating a shift of the equilibrium towards the low-spin six-coordinate component of the product mixture. This is in agreement with observations made when studying the temperature dependent spectra of liver microsomal cytochrome P450 in the presence of different substrates.[32] On releasing pressure the starting spectrum was obtained, which demonstrates the reversibility of the pressure-induced changes on the equilibrium. The presence of the externally added crown ether in solution, did not affect this pressure-dependent behaviour (Fig. S20, ESI†). The same behaviour we observed in the case of the complex with the covalently attached crown ether moiety, where we were able to demonstrate the existence of the equilibrium between the low-spin K[Fe^{II}(Porph)(DMSO)(O_2^-)] and high-spin K[Fe^{III}(Porph)(O_2^{2-})] species by means of different methods (Mössbauer, EPR, IR spectroscopy, ESI mass spectrometry, high-pressure kinetic measurements, DFT calculations).[5b,c] The quantification of such equilibrium constant is not possible to achieve since the spectra of the pure iron(II)-superoxo or pure iron(III)-peroxo forms are yet unknown, and there is no corresponding data available in the literature. Therefore, future studies will be required to tune this equilibrium such that it can be pushed completely in any of the two directions in order to independently characterize these two species.

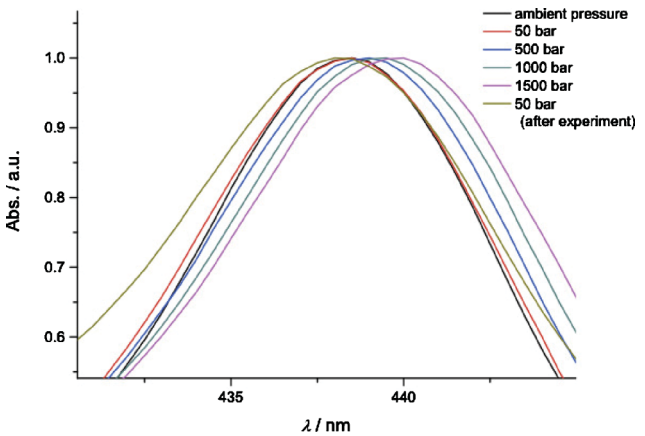

Fig. 6 UV/Vis spectra of K[Fe^{III}(tBuTPP)(O_2^{2-})] at different pressures in the presence of 0.1 M TBAP.

DFT calculations and correlations with experiments

To understand the possible influence of a nearby positive charge on the molecular and electronic structure of heme iron (su)peroxide adducts we performed DFT studies. The same B3LYP and

Table 2 Calculated B3PW91 (and B3LYP) relative energies (in kcal mol^{-1}) for end-on and side-on {Fe^{II}(porphyrin)$^{\bullet}$O$_2^{-\bullet}$} and {Fe^{II}(porphyrin)$^{\bullet}$O$_2^{-\bullet}$DMSO}

	Multiplicity	{Fe^{II}(porphyrin)$^{\bullet}$O$_2^{-\bullet}$}	{Fe^{II}(porphyrin)$^{\bullet}$O$_2^{-\bullet}$DMSO}
End-on	2	12.6 (8.2)	8.9 (3.5)[a]
	4	16.7 (14.0)	17.8[a]
	6	13.7 (13.9)	[b]
Side-on	2	21.9 (18.5)	[b]
	4	11.8 (12.9)	[b]
	6	0.0 (0.0)	[b]

[a] Compared to the energy of the free side-on sextet structure and a free DMSO ligand. [b] No complex with DMSO bound to the axial position was found on the PES.

B3PW91 levels of theory were used as in our previous study of the species with the crown ether moiety,[5b] for consistency. The optimized geometries of our computational models include the iron porphyrin core structure without the phenyl groups in *meso* positions, and the structures with and without coordinated DMSO are considered. Several different spin states (doublet, quartet and sextet) were considered for each structure (Table 2). Only the doublet and quartet states of the end-on structure bind DMSO with the doublet end-on structure being lowest in energy.

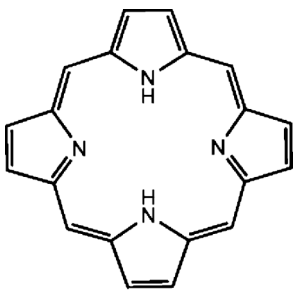

Porphyrin

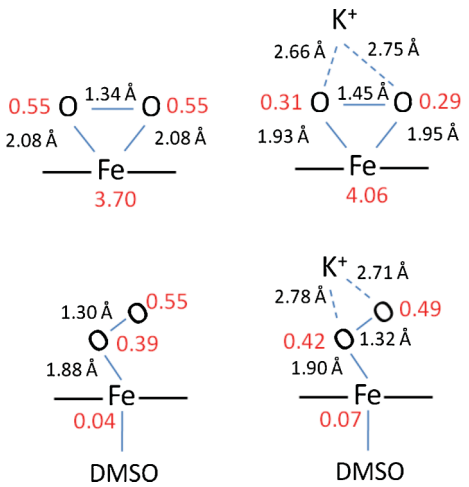

Scheme 4 Comparison of selected atomic distances and spin densities (red) for the calculated DMSO free sextet side-on porphyrin and the DMSO bound doublet end-on species of porphyrin (this work) and the model system with the covalently attached K$^+$-crown-ether moiety.[5b] Results were obtained at the B3PW91/BSI level of theory.

As in the previous study, the lowest energy structure found is the sextet high-spin side-on structure, in which the coordination site at the other side of the heme ring is vacant. The calculations suggest considerable superoxo character, as shown by the large spin densities on the both oxygen atoms (0.55, Scheme 4). The calculated O–O distance is 1.34 Å and the oxygen–oxygen bond lies above one of the N–N diagonals of the porphyrin ring. This is a typical superoxo O–O distance,[33] consistent with the calculated spin densities, though most experimental data on superoxide adducts of iron porphyrins strongly suggest that they have peroxo character[2] (an exception is an earlier ESR study describing such a species as Fe(II)-superoxo[34]). The Fe–O bond is somewhat elongated (Scheme 4), and the calculated structure of this side-on form can be understood in terms of weakly coordinated superoxide to high-spin Fe^{II}. Our previous DFT studies on the model system with the covalently attached crown ether including the chelated K$^+$ cation[5b] showed a larger peroxo character of the side-on sextet structure, with decreased spin-density on the oxygen atoms, longer O–O bond and shorter Fe–O bonds (Scheme 4). It seems that the nearby positive charge has a significant influence on the electronic structure of the side-on adduct. Indeed, a calculation on the simple model used here, but with an added 'naked' K$^+$ ion (no crown ether moiety) leads to results more similar to those in the previous study[5b] (reduced spin-density on the oxygen atoms 0.30, larger O–O bond distance 1.45 Å). Our thermodynamic and kinetic studies which show the greater stability of the (su)peroxo adduct in the case of the complex with the K$^+$-crown ether moiety are in agreement with the shortening of the Fe–O bonds caused by nearby positive charge. Additional stabilizing effect comes from the fact that the dissociation of axial ligands is to some extent sterically hindered by the bulkiness of the covalently linked crown ether (*vide supra*). It should be mentioned that based on our experiments, cations that are present in solution when KO_2 or Na_2O_2 are used as source of superoxide do not contribute to the product stability like the covalently attached cation moiety, which due to the steric proximity directly interacts with bound (su)peroxide inducing a stronger effect.

The end-on structure, which binds DMSO, is higher in energy than the side-on structure by 8.9 kcal mol^{-1} with B3PW91 or by 3.5 kcal mol^{-1} with B3LYP (Table 2). It has a doublet low-spin ground state with superoxo character. The spin density on the O atom nearer to Fe is 0.39 while on the distal one it is 0.55. The shortest Fe–O distance is 1.88 Å, and the O–O distance is 1.30 Å, similar to the distance of free superoxide.[27,33a] The Fe–O bond is significantly shorter than in the case of side-on structure (Scheme 4). The effect of the K$^+$-crown ether side chain on this end-on form

is negligible and does not influence its electronic structure, which remains to have low-spin Fe(II)-superoxo character (Scheme 4).

The energy difference between the side-on and end-on species suggests that the side-on structure is more favorable, but does not exclude the existence of equilibrium between them (3.5 kcal mol^{-1} energy difference obtained with B3LYP, Table 2). In the case of the model complex with covalently attached K^+-crown ether there was a smaller energy difference between these two isomeric forms.[5b] Our high-pressure experiments have shown the existence of the equilibrium in the product solution (*vide supra*). We should consider that the presence of the K^+ cations under experimental conditions in solution (from KO_2) lowers the energy difference between two forms, although not to that extent as in the case of the system with covalently attached K^+-crown ether side chain, but still favors their coexistence.

Collectively, the DFT data suggest that without nearby positive charge the reaction product has a character of a Fe^{II}-superoxo species in both side-on high-spin as well as end-on low-spin forms. The presence of the positive charge stabilizes the side-on high-spin adduct and changes its character into the Fe^{III}-peroxo species, whereas the Fe^{II}-superoxo character of the end-on low-spin isomer remains unchanged. One can speculate that if superoxide adduct would be produced in an experimental setup with no cations available in solution it would predominantly exhibit superoxo character (increased spin-density on the oxygen atoms, stronger O–O bond), but at the same time significantly decreased stability (weaker Fe–O bond). Such experimental conditions can be achieved by *in situ* radiolytic cryoreduction of heme Fe^{II}–O_2 adducts.[3] Interestingly, such $\{Fe–O_2\}^-$ products have usually been described as end-on peroxo species, although based on the observed O–O distance[3b,c] and quantum chemical calculations they are best interpreted as Fe^{II}–O_2^-.[33a,35] Only Davydov *et al.* clearly classified the primary reduction product of monomeric oxy-hemoglobin (oxy-GMH3) from *Glycera dibranchiata* as Fe^{II}-superoxo based on EPR/ENDOR experiments.[3a] They also suggest that the internal redox transition to peroxo/hydroperoxo-ferric intermediates is driven by H-bonding/proton donation by the environment,[3a] which, based on our findings, can be interpreted as peroxo form stabilization by adjacent positive charge.

Conclusion

Based on our investigations of the superoxide reactions with Fe^{II} porphyrins with and without covalently attached crown ether moiety and with deliberately added crown ether we can conclude the following: (a) superoxide binds reversibly to Fe^{II} porphyrins in DMSO independently on the general existence of crown ether, (b) in DMSO solution with an excess of superoxide, the product (su)peroxo species generates the starting Fe^{II} complex upon controlled addition of a proton source, also independent on the presence of the crown ether moiety, (c) to a certain extent, the crown ether side chain favors the low-spin six-coordinate form of the Fe^{II} porphyrin in the solution, (d) since generation of the high-spin five-coordinate Fe^{II} species is the actual activation step towards substitution and subsequent inner-sphere electron transfer, the superoxide binding (k_{on}) is approximately one order of magnitude slower when crown ether is covalently attached to porphyrin, whereas externally added crown ether does not influence the rate determining step, (e) by preventing the axial ligand dissociation covalently attached crown ether slows down the superoxide release from the product (su)peroxo species (resulting in a decrease of k_{off} by two orders of magnitude), (f) the more prominent effect of attached crown ether on the superoxide dissociation (k_{off}) than on the DMSO dissociation (k_{on}) suggests that the positive charge of chelated K^+ additionally prevents the superoxide release, (g) these effects of the crown ether side chain on k_{on} and k_{off} result in the ten times larger superoxide binding constant and make the product (su)peroxo complex significantly more stable, whereas external addition of crown ether does not bring any stabilization, (h) due to this higher stability, detailed spectroscopic studies on the (su)peroxo complex with the crown ether side chain could be performed, demonstrating the existence of the redox tautomerism between the end-on Fe^{II}-superoxo and side-on Fe^{III}-peroxo forms, which is supported by DFT calculations, (i) the lower solubility and stability of the (su)peroxo complex without crown ether moiety did not allow detailed spectroscopic characterization of its nature, however, DFT calculations demonstrate that without nearby positive charge the reaction product has the Fe^{II}-superoxo character in both side-on high-spin as well as end-on low-spin forms. These findings are important for understanding the real nature of the corresponding biologically relevant (su)peroxo intermediaries of heme-containing enzymes involved in activation of molecular oxygen and hydrogen peroxide, because they show that the nature and electronic structure of these intermediates can be tuned not only by axial ligand coordination but also by the charge of a surrounding of an iron heme center in the active site of an enzyme. Our kinetic and thermodynamic studies quantify the effect of semi-confined environment around iron center, caused by the covalently attached crown-ether, on its reactivity toward axial ligands in general, and superoxide in particular. The results obtained in this investigation represent a motivating foundation for future studies towards the understanding of the effects that might be caused by the solvent, a *trans* ligand, and possible involvement of coordinated (su)peroxide in hydrogen bonding or electrostatic interactions, on the structure and electronic properties of the heme iron-superoxide adducts and their reactivity towards different organic substrates of biological and synthetic importance.

Acknowledgements

This work was supported by the Deutsche Forschungsgemeinschaft through SFB 583 "Redox-active metal complexes" (K. D., A. Z., N. J., I. I. B). J. O. acknowledges receipt of an EU Marie Curie Fellowship (Project "Modelling CYPs").

References

1 (*a*) I. Schlichting, J. Berendzen, K. Chu, A. M. Stock, S. A. Maves, D. E. Benson, R. M. Sweet, D. Ringe, G. A. Petsko and S. G. Sligar, *Science*, 2000, **287**, 1615; (*b*) D. L. Wertz and J. S. Valentine, *Struct. Bonding*, 2000, **97**, 37; (*c*) E. Kim, E. E. Chufan, K. Kamaraj and K. D. Karlin, *Chem. Rev.*, 2004, **104**, 1077.

2 (*a*) E. McCandlish, A. R. Miksztal, M. Nappa, A. Q. Sprenger, J. S. Valentine, J. D. Stong and T. G. Spiro, *J. Am. Chem. Soc.*, 1980, **102**, 4268; (*b*) J. N. Burstyn, J. A. Roe, A. R. Miksztal, B. A. Shaevitz, G. Lang and J. S. Valentine, *J. Am. Chem. Soc.*, 1988, **110**, 1382; (*c*) E. E. Chufan and K. D. Karlin, *J. Am. Chem. Soc.*, 2003, **125**, 16160; (*d*) M. Selke, M. F. Sisemore and J. S. Valentine, *J. Am. Chem. Soc.*, 1996, **118**, 11692.

3 (*a*) R. Davydov, J. D. Satterlee, H. Fujii, A. Sauer-Masarwa, D. H. Busch and B. M. Hoffman, *J. Am. Chem. Soc.*, 2003, **125**, 16340; (*b*) H.-P. Hersleth, Y.-W. Hsiao, U. Ryde, C. H. Goerbitz and K. K. Andersson, *Biochem. J.*, 2008, **412**, 257; (*c*) M. Unno, H. Chen, S. Kusama, S. Shaik and M. Ikeda-Saito, *J. Am. Chem. Soc.*, 2007, **129**, 13394.
4 J.-G. Liu, T. Ohta, S. Yamaguchi, T. Ogura, S. Sakamoto, Y. Maeda and Y. Naruta, *Angew. Chem., Int. Ed.*, 2009, **48**, 9262.
5 (*a*) K. Duerr, B. P. Macpherson, R. Warratz, F. Hampel, F. Tuczek, M. Helmreich, N. Jux and I. Ivanović-Burmazović, *J. Am. Chem. Soc.*, 2007, **129**, 4217; (*b*) K. Duerr, J. Olah, R. Davydov, M. Kleimann, J. Li, N. Lang, R. Puchta, E. Huebner, T. Drewello, J. N. Harvey, N. Jux and I. Ivanović-Burmazović, *Dalton Trans.*, 2010, **39**, 2049; (*c*) K. Duerr, N. Jux, A. Zahl, R. van Eldik and I. Ivanović-Burmazović, *Inorg. Chem.*, 2010, **49**, 11254.
6 I. Rosenthal, *J. Labelled Compd. Radiopharm.*, 1976, **12**, 317.
7 A. Zahl, A. Neubrand, S. Aygen and R. van Eldik, *Rev. Sci. Instrum.*, 1994, **65**, 882.
8 J. Maigut, R. Meier, A. Zahl and R. van Eldik, *Inorg. Chem.*, 2007, **46**, 5361.
9 I. Ivanović-Burmazović, M. S. A. Hamza and R. van Eldik, *Inorg. Chem.*, 2006, **45**, 1575.
10 (*a*) G.-F. Liu, M. Filipović, F. W. Heinemann and I. Ivanović-Burmazović, *Inorg. Chem.*, 2007, **46**, 8825; (*b*) G.-F. Liu, M. Filipović, I. Ivanović-Burmazović, F. Beuerle, P. Witte and A. Hirsch, *Angew. Chem., Int. Ed.*, 2008, **47**, 3991.
11 (*a*) M. Spitzer, F. Gartig and R. van Eldik, *Rev. Sci. Instrum.*, 1988, **59**, 2092; (*b*) K. F. Fleischmann, G. E. Conze, R. D. Stranks and H. Kelm, *Rev. Sci. Instrum.*, 1974, **45**, 1427.
12 Jaguar, version 6.0, Schrödinger, LLC, New York, NY, 2005.
13 J. P. Hay and W. R. Wadt, *J. Chem. Phys.*, 1985, **82**, 299.
14 The LACV3P basis set is a triple-zeta contraction of the LACVP basis set developed and tested at Schrödinger, Inc.
15 J. K. M. Sanders, N. Bampos, Z. Clyde-Watson, S. L. Darling, J. C. Hawley, H.-J. Kim, C. C. Mak and S. J. Webb, in *The Porphyrin Handbook*, ed. K. Kadish, K. Smith and R. Guilard, Academic Press, New York, 2003, vol. 3.
16 (*a*) R. C. Parmely and H. M. Goff, *J. Inorg. Biochem.*, 1980, **12**, 269; (*b*) A. Shirazi and H. M. Goff, *J. Am. Chem. Soc.*, 1982, **104**, 6318.
17 F. A. Walker, *The Porphyrin Handbook*, Academic Press, New York, 2003, vol. 5.
18 R. Lange, C. Larroque and P. Anzenbacher, *Eur. J. Biochem.*, 1992, **207**, 69.
19 B. Li, R.-J. Wei, J. Tao, R.-B. Huang and L.-S. Zheng, *Inorg. Chem.*, 2010, **49**, 745, and references therein.
20 J. Mikškovska, J. Norstrom and R. W. Larsen, *Inorg. Chem.*, 2005, **44**, 1006.
21 K. Hereman, in *High-pressure Chemistry and Biochemistry*, ed. R. van Eldik and J. Jonas, D. Reidel Publishing Co., Dordrecht, Holland, 1987.
22 (*a*) R. van Eldik, T. Asano and W. le Noble, *Chem. Rev.*, 1989, **89**, 549; (*b*) R. R. Hung and J. J. Grabowski, *J. Am. Chem. Soc.*, 1992, **114**, 351.
23 A. Franke, N. Hessenauer-Ilicheva, D. Meyer, G. Stochel, W. D. Woggon and R. van Eldik, *J. Am. Chem. Soc.*, 2006, **128**, 13611.
24 (*a*) G. Hui Bon Hoa and M. C. Marden, *Eur. J. Biochem.*, 1982, **124**, 311; (*b*) D. R. Davydov, G. Hui Bon Hoa and J. A. Peterson, *Biochemistry*, 1999, **38**, 751.
25 H. N. Miras, E. F. Wilson and L. Cronin, *Chem. Commun.*, 2009, 1297, and references therein.
26 D.-H. Chin, G. Jr. Chiericato, E. J. Jr. Nanni and D. T. Sawyer, *J. Am. Chem. Soc.*, 1982, **104**, 1296.
27 D. T. Sawyer and J. S. Valentine, *Acc. Chem. Res.*, 1981, **14**, 393.
28 E. E. Chufan and K. D. Karlin, *J. Am. Chem. Soc.*, 2003, **125**, 16160.
29 G. Palmer in *Physical Methods in Bioinorganic Chemistry*, ed. L. Que, Jr., University Science Books, Sausalito, CA, 2000.
30 K. M. Kadish, G. Larson, D. Lexa and M. Momenteau, *J. Am. Chem. Soc.*, 1975, **97**, 282.
31 M. C. R. Symons, G. W. Eastland and L. R. Denny, *J. Chem. Soc., Faraday Trans. 1*, 1980, **76**, 1868.
32 H. Rein, O. Ristau, J. Friedrich, G.-R. Jänig and K. Ruckpaul, *FEBS Lett.*, 1977, **75**, 19.
33 (*a*) M. Pedio, Z. Y. Wu, M. Benfatto, A. Mascaraque, E. Michel, C. Ottaviani, C. Crotti, M. Peloi, M. Zacchigna and C. Comicioli, *Phys. Rev. B: Condens. Matter*, 2002, **66**, 144109/144101/144104; (*b*) C. J. Cramer, W. B. Tolman, K. H. Theopold and A. L. Rheingold, *Proc. Natl. Acad. Sci. U. S. A.*, 2003, **100**, 3635.
34 V. K. Kol'tover, O. I. Koifman, A. M. Khenkin and A. A. Shteinman, *Izv. Akad. Nauk SSSR, Ser. Khim.*, 1978, 1690.
35 E. G. Kovaleva and J. D. Lipscomb, *Science*, 2007, **316**, 453.